Environ. Sci. Technol. **2003**, *37,* 2442−2452

High-Order, Direct Sensitivity Analysis of Multidimensional Air Quality Models

AMIR HAKAMI, M. TALAT ODMAN, AND ARMISTEAD G. RUSSELL*

School of Civil and Environmental Engineering, Georgia Institute of Technology, Atlanta, Georgia 30332-0512

A direct sensitivity analysis technique is extended to calculate higher-order sensitivity coefficients in three-dimensional air quality models. The time evolution of sensitivity coefficients of different order is followed alongside that of the concentrations. Calculation of higher-order sensitivity coefficients requires few modifications to the original (first-order) sensitivity modules and is carried out efficiently and with minimal computational overhead. The modeling results (first-, second-, and third-order sensitivity coefficients) for an ozone episode in central California are shown and discussed. Second-order sensitivity coefficients of ozone concentration with respect to domain-wide NO emissions show reasonable agreement with brute-force results and exhibit less noisy behavior. By using second-order sensitivity coefficients the nonlinear responses are better captured and described. For a Taylor series projection from the base case, including the second-order term improves the accuracy. In general, higher-order sensitivity analysis shows a noticeable improvement in terms of accuracy over the conventional first-order analysis. Of particular interest, second-order sensitivity analysis is better equipped to address the nonlinear behavior around the peak ozone in NO_x-rich plumes.

Introduction

Air Quality Models (AQMs) are an indispensable part of air quality management and planning, as they are the only viable tools for evaluating the atmospheric response to different control measures. These responses can be predicted through different sensitivity analysis techniques, where sensitivity coefficients (derivatives) to various model input parameters (e.g., emission rates, initial or boundary conditions, and rate constants) are calculated. Numerous methods for sensitivity analysis have been developed and investigated. The brute-force (finite difference) method is the most widely used technique (*1*−*4*), where the sensitivities are calculated by one-at-a-time perturbation of model inputs or parameters. The implementation of the brute-force method is easy and straightforward but becomes prohibitively cumbersome as the number of sensitivity parameters increases. Brute-force sensitivity for a small perturbation is prone to numerical noise, and it is not apparent to how large a perturbation the calculated sensitivity applies.

A number of methods have been developed for local sensitivity analysis, i.e., to calculate partial derivatives about the nominal value of the sensitivity parameter. Green's Function Method (GFM) (*5, 6*) and its variations (*7, 8*) have been applied to chemical kinetic systems and atmospheric chemistry. GFM is computationally costly but becomes efficient as the number of sensitivity parameters approaches the number of chemical species. Automatic DIfferentiation in FORtran (ADIFOR) (*9*) is another technique that has been applied to subsystems of AQMs (*10, 11*). To calculate the sensitivity coefficients, ADIFOR follows the sequence of elementary operations in the computer code automatically, but it does not take advantage of the existing program structure.

Another group of sensitivity analysis techniques rely on direct solution to the sensitivity equations. In the Direct Method (DM) (*12*), sensitivity equations are derived from, and solved together with, the main governing equations of the model. The Decoupled Direct Method (DDM) (*13, 14*) provides more stability and computational efficiency than the DM by integrating the sensitivity equations decoupled from the original model equations. DDM equations follow the same structure as the model equations, making its implementation straightforward. DDM is efficient for large numbers of sensitivity parameters and is not subject to numerical noise for small ranges. DDM has been applied to different chemical kinetic systems, including zero-dimensional atmospheric models (*15*−*17*). Due to its computational efficiency, DDM remains the only local sensitivity analysis technique that has been extensively used in three-dimensional AQMs (*18*−*23*).

DDM is typically used for calculation of the first-order sensitivity coefficients, while its application for calculating second-order coefficients has been suggested and explored (*14, 24, 25*). In the context of air quality modeling, sensitivity analysis has been mainly limited to calculation of the first-order sensitivity coefficients. Second-order sensitivity analysis has been applied to box models (*26, 27*), mainly with the use of computationally expensive GFM (*28*). Atmospheric models, due to the chemistry, may exhibit a nonlinear response that cannot be captured by first-order sensitivity analysis. In this paper, a High-order, Decoupled Direct Method (HDDM) for sensitivity analysis is developed to efficiently calculate the second- (and higher) order local sensitivity coefficients in multidimensional AQMs. Calculation of these additional coefficients allows for higher-order sensitivity analysis, hence capturing nonlinearities in atmospheric responses. The method is derived from the more conventional DDM-3D (*18*), is computationally efficient, and calculates the higher-order coefficients with minimal additional overhead. HDDM can be efficiently applied to different sensitivity parameters, e.g., emission rates, initial and boundary conditions, dry deposition velocities, etc. It is also capable of calculating cross sensitivities, i.e., higher-order sensitivity coefficients with respect to more than one independent variable. The method is implemented in the Multiscale Air Quality SImulation Platform [MAQSIP (*29*)] and applied to the SARMAP (*30*) domain during August 2−6, 1990 episode. While HDDM is developed for general calculation of higher-order sensitivity coefficients, the results here are mainly for the second-order results with less emphasis on third-order coefficients.

Methodology

Atmospheric transport and chemistry in AQMs are described by the Atmospheric Diffusion Equation (ADE) (*31*):

$$\frac{\partial C_i}{\partial t} = -\nabla(\mathbf{u}C_i) + \nabla(\mathbf{K}\nabla C_i) + R_i + E_i \qquad (1)$$

$$(i = 1,2,...,N)$$

* Corresponding author phone: (404)894-3079; fax: (404)894-8266; e-mail: trussell@ce.gatech.edu.

10.1021/es020677h CCC: $25.00
Published on Web 05/03/2003

where **u** is the three-dimensional wind field, **K** is the turbulent diffusivity tensor, and N is the total number of chemical species. C_i, E_i, and R_i are the grid cell average concentration, emission rate, and chemical reaction rate of species i, respectively. Integration of the ADE is carried out numerically using the method of operator splitting and subject to specific initial and boundary conditions (*31*):

$$\text{IC:}\quad C_i = C_{0_i} \tag{2a}$$

$$\text{BCs:}\quad \mathbf{u}C_i - \mathbf{K}\nabla C_i = \mathbf{u}C_{b_i} \tag{2b}$$

$$-\nabla C_i = 0 \tag{2c}$$

$$v_{g_i}C_i - K_{zz}\frac{\partial C_i}{\partial z} = E_{0_i} \tag{2d}$$

where C_{b_i}, C_{0_i}, v_{g_i}, and E_{0_i} are the boundary and initial concentrations, dry deposition velocity, and surface level emission rate of species i, respectively.

The first-order (linear) local sensitivity coefficient is defined as $s_{ij}^{(1)} = \partial C_i/\partial p_j$, where $s_{ij}^{(1)}$ is the first-order sensitivity coefficient of species i, with respect to sensitivity parameter p_j. These local sensitivities depend on the magnitude of the sensitivity parameter and offer little comparative basis. Therefore, the seminormalized local first-order sensitivity coefficient, $S_{ij}^{(1)}$, is defined as

$$S_{ij}^{(1)} = \tilde{p}_j\frac{\partial C_i}{\partial p_j} = \tilde{p}_j\frac{\partial C_i}{\partial(\epsilon_j\tilde{p}_j)} = \frac{\partial C_i}{\partial \epsilon_j} \tag{3}$$

where $\tilde{p}_j$ is the unperturbed field (the nominal value of p_j, i.e., the values used in the simulation), and ϵ_j is a scaling variable ($p_j = \epsilon_j\tilde{p}_j$) with a nominal value of 1. Differentiating eq 1 results in the following DDM equation for the first-order sensitivity coefficients (*18*):

$$\frac{\partial S_{ij}^{(1)}}{\partial t} = -\nabla(\mathbf{u}S_{ij}^{(1)}) + \nabla(\mathbf{K}\nabla S_{ij}^{(1)}) + \mathbf{J}_i\mathbf{S}_j^{(1)} + \frac{\partial R_i}{\partial \epsilon_j}\delta_{5j_1} + \tilde{\mathrm{E}}_i\delta_{1j_1}\delta_{ij_2} - \nabla(\tilde{\mathbf{u}}C_i)\delta_{3j_1} + \nabla(\tilde{\mathbf{K}}\nabla C_i)\delta_{4j_1} \tag{4}$$

Sensitivity boundary conditions can be written as (*18*)

$$\text{IC:}\quad S_{ij}^{(1)} = \tilde{C}_{0_i}\delta_{0j_1}\delta_{ij_2} \tag{5a}$$

$$\text{BCs:}\quad \mathbf{u}S_{ij}^{(1)} - \mathbf{K}\nabla S_{ij}^{(1)} = \mathbf{u}\tilde{C}_{b_i}\delta_{2j_1}\delta_{ij_2} + \tilde{\mathbf{u}}C_{bi}\delta_{3j_1} - \tilde{\mathbf{u}}C_i\delta_{3j_1} + \tilde{\mathbf{K}}\nabla C_i\delta_{4j_1} \tag{5b}$$

$$-\nabla S_{ij}^{(1)} = 0 \tag{5c}$$

$$v_{g_i}S_{ij}^{(1)} - K_{zz}\frac{\partial S_{ij}^{(1)}}{\partial z} = -\tilde{v}_{g_i}C_i\delta_{6j_1}\delta_{ij_2} + \tilde{K}_{zz}\frac{\partial C_i}{\partial z}\delta_{4j_1} + \tilde{E}_{0_i}\delta_{1j_1}\delta_{ij_2} \tag{5d}$$

$\mathbf{J}_i$ is the ith row vector in the Jacobian matrix, $\mathbf{J}$ ($J_{ik} = \partial R_i/\partial C_k, k = 1,2,...,N$), of the reaction rates. $\mathbf{S}_j^{(1)}$ is the vector of the first-order coefficients for sensitivity parameter p_j, and δ_{ij} is the Kronecker delta function. Subscript j_1 denotes the type of the sensitivity parameter p_j, with indices 0−6 referring to initial condition, emission rate, boundary condition, wind field, diffusivity, rate constant, and dry deposition sensitivity parameters, respectively. Subscript j_2, on the other hand, refers to the species with respect to which a dry deposition, initial or boundary condition, or emissions sensitivity is calculated. For example, if ozone is the first species in the chemical mechanism (i.e., it is given the order number 1), and the sensitivities are calculated with respect to its initial condition, then j_1 and j_2 are 0 and 1, respectively. For sensitivity of ozone to the emissions of NO (e.g. with the species rank of 5), j_1 and j_2 are 1 and 5, respectively. Therefore, only delta functions δ_{1j_1} and δ_{5j_2} are nonzero. Again, $\tilde{C}_{b_i}$, $\tilde{C}_{0_i}$, $\tilde{v}_{g_i}$, $\tilde{E}_{0_i}$, $\tilde{\mathbf{u}}$, and $\tilde{\mathbf{K}}$ are nominal values of the corresponding parameters and, therefore, are treated as constants.

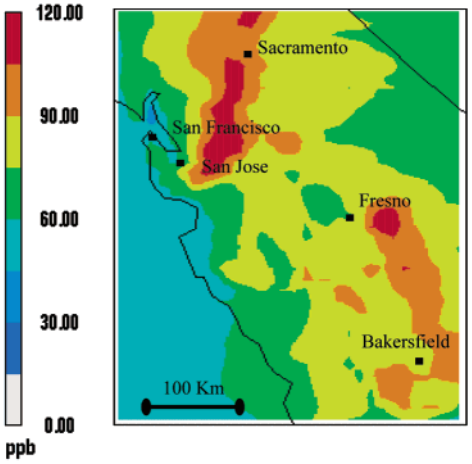

FIGURE 1. Average ozone concentration at the time of episode's peak ozone, 3−4 p.m. local time, August 2nd.

Equation 4 has a very similar structure to eq 1 (ADE), and for the most part can be integrated by the same numerical routines. Therefore, the DDM implementation can be achieved with minimal effort and without substantial changes in the AQM structure. Unlike the ADE, sensitivity equations, when decoupled from concentrations are linear with respect to sensitivity coefficients. At each time step, sensitivity integration is carried out separately from, and only after, concentrations are integrated.

The main computational burden of sensitivity calculations lies in the integration of chemical sensitivity rates. In the operator splitting scheme, these rates are described by the following set of ordinary differential equations (*18*)

$$\frac{\partial \mathbf{S}_j^{(1)}}{\partial t} = \mathbf{J}\mathbf{S}_j^{(1)} + \frac{\partial \mathbf{R}}{\partial \epsilon_j} \tag{6}$$

where **R** is the vector of chemical reaction rates. Chemical sensitivity ODEs in DDM-3D are discretized (for time step $n+1$ in terms of the solution at time step n) as

$$\frac{\mathbf{S}_j^{(1)^{n+1}} - \mathbf{S}_j^{(1)^n}}{\Delta t} = \mathbf{J}_{\bar{\mathbf{C}}}\left(\frac{\mathbf{S}_j^{(1)^{n+1}} + \mathbf{S}_j^{(1)^n}}{2}\right) + \frac{\partial \mathbf{R}_{\bar{\mathbf{C}}}}{\partial \epsilon_j}\delta_{5j_1} \tag{7}$$

where $\bar{\mathbf{C}} = (\mathbf{C}^{n+1} + \mathbf{C}^n)/2$. Solving this linear system results in

$$\mathbf{S}_j^{(1)^{n+1}} = \left(\mathbf{I} - \frac{\Delta t}{2}\mathbf{J}_{\bar{\mathbf{C}}}\right)^{-1}\left\{\left(\mathbf{I} + \frac{\Delta t}{2}\mathbf{J}_{\bar{\mathbf{C}}}\right)\mathbf{S}_j^{(1)^n} + \Delta t\frac{\partial \mathbf{R}_{\bar{\mathbf{C}}}}{\partial \epsilon_j}\delta_{5j_1}\right\} \tag{8}$$

The Jacobian matrix is independent of sensitivities, and the required matrix factorization (the main computational cost) is carried out only once for all sensitivity parameters at each time step and grid. This feature enables DDM-3D to calculate sensitivity coefficients for a large number of sensitivity parameters in an efficient manner.

Equations for the second-order sensitivity coefficients can be derived using a similar procedure. Differentiating eq 4

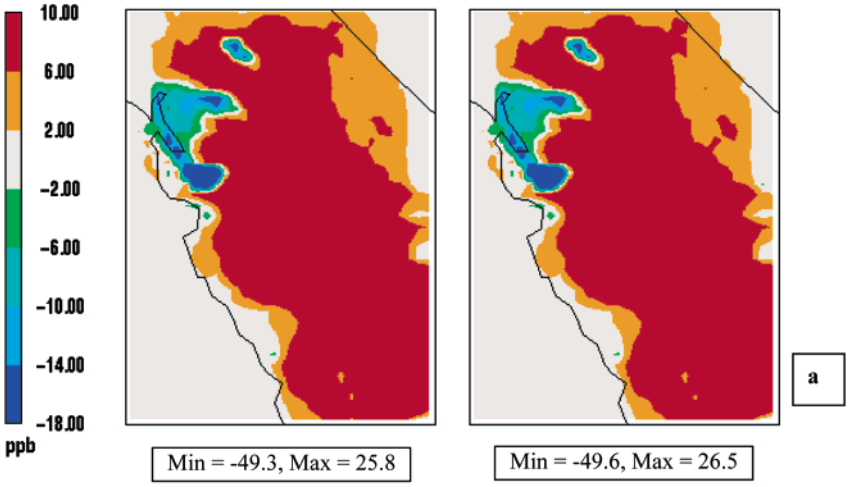
10.00
6.00
2.00
−2.00
−6.00
−10.00
−14.00
−18.00
ppb
Min = -49.3, Max = 25.8
Min = -49.6, Max = 26.5
a

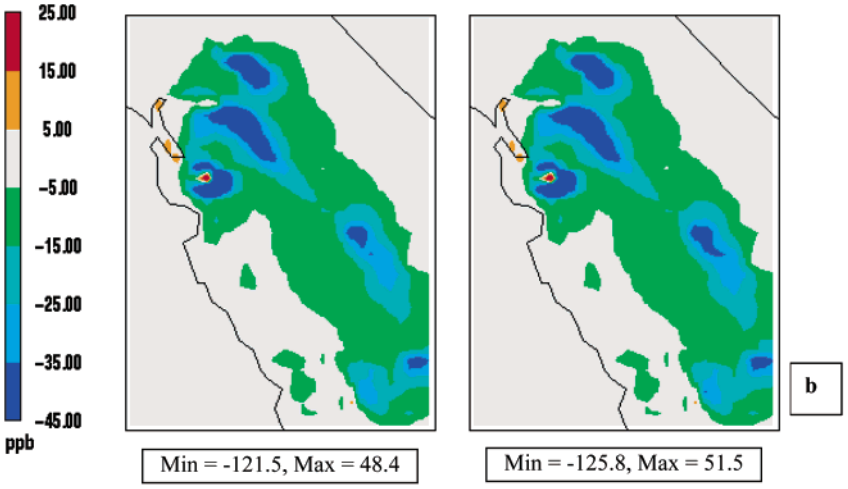
25.00
15.00
5.00
−5.00
−15.00
−25.00
−35.00
−45.00
ppb
Min = -121.5, Max = 48.4
Min = -125.8, Max = 51.5
b

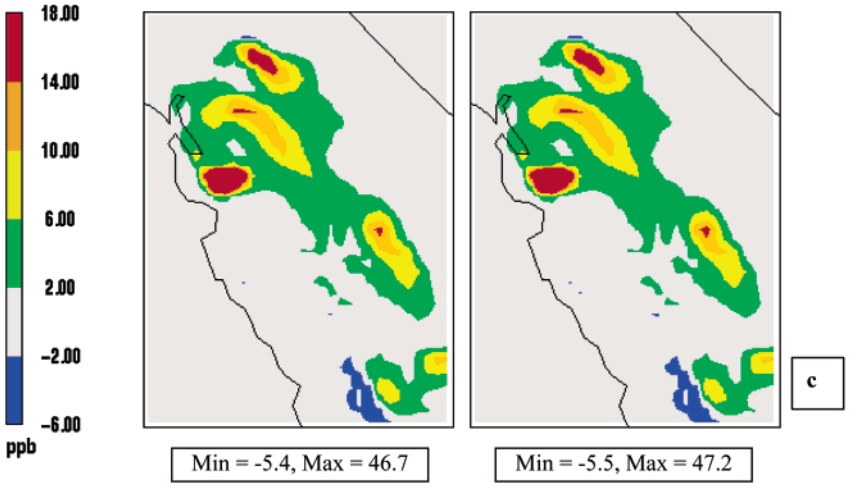
18.00
14.00
10.00
6.00
2.00
−2.00
−6.00
ppb
Min = -5.4, Max = 46.7
Min = -5.5, Max = 47.2
c

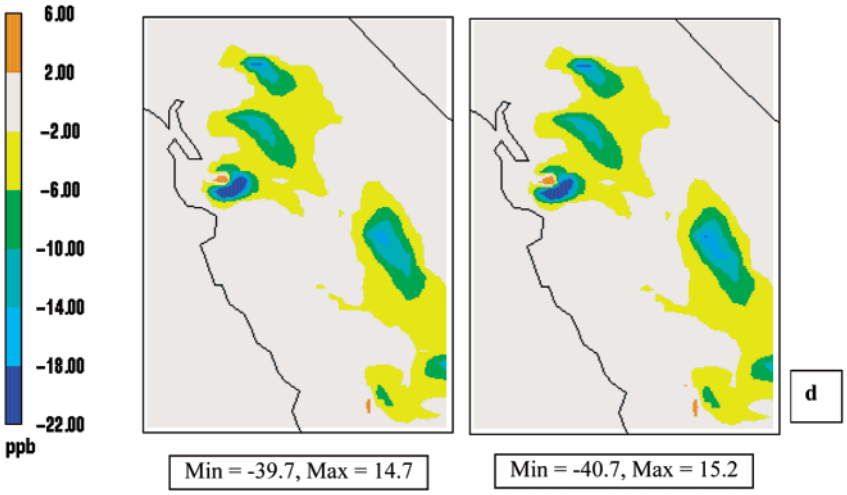

FIGURE 2. Comparison of (H)DDM (right) vs brute-force (left) ozone sensitivity coefficients: (a) first-order to domain-wide NO emissions, (b) second-order to domain-wide NO emissions, (c) first-order to domain-wide VOC emissions, and (d) second-order to domain-wide VOC emissions. All the plots show average values for the hour of peak ozone concentration (2−3 p.m.) on August 4th. Brute-force coefficients are calculated using a central difference approximation and 10% perturbation (±) in domain-wide emissions.

with respect to sensitivity parameter p_j (the same parameter as for first-order calculations) gives

$$\frac{\partial S_{ij}^{(2)}}{\partial t} = -\nabla(\mathbf{u}S_{ij}^{(2)}) + \nabla(\mathbf{K}\nabla S_{ij}^{(2)}) + \mathbf{J}_i\mathbf{S}_j^{(2)} + \mathbf{J}_{i,S^{(1)}}^{*}\mathbf{S}_j^{(1)} + 2\frac{\partial}{\partial \epsilon_j}(\mathbf{J}_{i,\bar{C}}\mathbf{S}_j^{(1)})\delta_{5j_1} - 2\nabla(\tilde{\mathbf{u}}S_{ij}^{(1)})\delta_{3j_1} + 2\nabla(\tilde{\mathbf{K}}\nabla S_{ij}^{(1)})\delta_{4j_1} \quad (9)$$

with the following initial and boundary conditions:

$$\text{IC:}\quad S_{ij}^{(2)} = 0 \quad (10a)$$

$$\text{BCs:}\quad \mathbf{u}S_{ij}^{(2)} - \mathbf{K}\nabla S_{ij}^{(2)} = -2\tilde{\mathbf{u}}S_{ij}^{(1)}\delta_{3j_1} + 2\tilde{\mathbf{K}}\nabla S_{ij}^{(1)}\delta_{4j_1} \quad (10b)$$

$$-\nabla S_{ij}^{(2)} = 0 \quad (10c)$$

$$v_{g_i}S_{ij}^{(2)} - K_{zz}\frac{\partial S_{ij}^{(2)}}{\partial z} = -2\tilde{v}_{g_i}S_{ij}^{(1)}\delta_{6j_1}\delta_{ij_2} + 2\tilde{K}_{zz}\frac{\partial S_{ij}^{(1)}}{\partial z}\delta_{4j_1} \quad (10d)$$

where $\mathbf{S}_j^{(2)}$ is the vector of second-order coefficients, $S_{ij}^{(2)}$. $\mathbf{J}_{S^{(1)}}^{*}$, a square matrix, is the augmented chemical rate Jacobian, and $\mathbf{J}_{i,S^{(1)}}^{*}$ refers to the ith row vector of $\mathbf{J}_{S^{(1)}}^{*}$. Since the maximum effective order of the atmospheric reactions is generally two, $\mathbf{J}_{S^{(1)}}^{*}$ will have the same structure as $\mathbf{J}_{\bar{C}}$ with all entries for first-order and effective first-order reactions excluded. Subscript $S^{(1)}$ indicates that instead of concentrations, first-order sensitivity coefficients are used to evaluate the augmented Jacobian matrix. For consistency, all augmented Jacobians (as well as lower-order coefficients) are evaluated using the average of the sensitivity coefficients at the new and old time steps. Note that second-order coefficients are decoupled from the temporal evolution of the concentrations and first-order coefficients. Also, first-order terms/processes such as initial and boundary conditions and emissions do not appear directly in the second-order sensitivity equations but indirectly affect the calculations through the concentrations and first-order sensitivity coefficients.

In the above derivation, for the purpose of simplicity, the second-order sensitivity coefficient is calculated with respect to the same parameter (p_j) as the first-order one, leading to the second-order derivative with respect to only one independent parameter. Cross sensitivities (i.e., second-order derivatives with respect to two different sensitivity parameters) can be formulated in the same fashion. Calculation of the cross-sensitivities can be implemented in the model similarly, but additional information must be stored. Chemistry discretization corresponding to eq 9 is written as

$$\mathbf{S}_j^{(2)^{n+1}} = \left(\mathbf{I} - \frac{\Delta t}{2}\mathbf{J}_{\bar{C}}\right)^{-1}\left[\left(\mathbf{I} + \frac{\Delta t}{2}\mathbf{J}_{\bar{C}}\right)\mathbf{S}_j^{(2)^n} + \Delta t\mathbf{J}_{S^{(1)}}^{*}\bar{\mathbf{S}}_j^{(1)} + 2\Delta t\frac{\partial}{\partial \epsilon_j}(\mathbf{J}_{\bar{C}}\bar{\mathbf{S}}_j^{(1)})\delta_{5j_1}\right] \quad (11)$$

where $\bar{\mathbf{S}} = (\mathbf{S}^{n+1} + \mathbf{S}^n)/2$. The required matrix factorization is again independent of any sensitivity coefficient and needs to be carried out only once for first- and second-order coefficients of all sensitivity parameters. This ensures a highly efficient calculation of the second-order sensitivity coefficients. The method explained above can be generalized to calculate higher-order sensitivity coefficients. For instance, for the sensitivity to emission rates (the most usual case), higher-order sensitivity coefficients (of order m, $m \geq 2$) can be calculated as

$$\frac{\partial \mathbf{S}_j^{(m)}}{\partial t} = -\nabla(\mathbf{u}\mathbf{S}_j^{(m)}) + \nabla(\mathbf{K}\nabla\mathbf{S}_j^{(m)}) + \mathbf{J}\mathbf{S}_j^{(m)} + \sum_{k=1}^{m-1}\binom{m-1}{k}\mathbf{J}_{S^{(k)}}^{*}\mathbf{S}_j^{(m-k)} \quad (12)$$

here $\mathbf{S}_j^{(m)}$ is the vector of mth order sensitivity coefficients, and $\binom{m}{k}$ is the kth binomial coefficient of order m. Chemistry discretization may be formulated as

$$\mathbf{S}_j^{(m)^{n+1}} = \left(\mathbf{I} - \frac{\Delta t}{2}\mathbf{J}_{\bar{C}}\right)^{-1}\left[\left(\mathbf{I} + \frac{\Delta t}{2}\mathbf{J}_{\bar{C}}\right)\mathbf{S}_j^{(m)^n} + \Delta t\sum_{k=1}^{m-1}\binom{m-1}{k}\mathbf{J}_{S^{(k)}}^{*}\bar{\mathbf{S}}_j^{(m-k)}\right] \quad (13)$$

Similar to the case of the second-order calculations, higher-order sensitivity coefficients are solved decoupled from concentrations and all lower coefficients.

Results and Discussion

Here, HDDM is applied in MAQSIP (*29*) using the CB-IV (*32*) chemical mechanism. The modeling is conducted over the

SARMAP domain, consisting of uniform 12-km horizontal grids (32 columns and 39 rows) and 15 vertical layers, and for the August 2−6, 1990 episode (*30*). In this version of MAQSIP, the Bott advection scheme (*33*) was used for horizontal transport, with proper adjustments for sensitivity calculations (*23*). MAQSIP originally used modified versions of the hybrid (*34*) and QSSA (*35*) solvers for the integration of chemical rates. Those versions were found to be inaccurate for brute-force estimations and were replaced by RODAS from the family of Rosenbrock solvers (*36*). RODAS is shown to perform very efficiently for high accuracy applications (*37*). For lower degree of accuracy but faster computation, the hybrid solver from California/Carnegie Institute of Technology (CIT) model (*38*) was imported into MAQSIP and was found to provide suitable accuracy.

Figure 1 shows the domain and spatial ozone distribution at the time of the episode's peak ozone concentration. The episode's peak ozone occurs in the plume from the San Francisco Bay area during the late afternoon hours of August 2nd. Daily peak ozone concentrations for August 4−6 occur downwind of Fresno. Figure 2a compares the peak-time first-order sensitivity coefficient of ozone to domain-wide NO emissions for the brute-force and DDM-3D calculations on August 4th. Sensitivity of ozone to NO is chosen as a benchmark for higher-order sensitivity analysis because it exhibits one of the most dynamic and nonlinear atmospheric responses. In this case, the brute-force sensitivities are calculated as central difference approximations using a 10% perturbation ($\Delta\epsilon = 0.1$, or $\Delta p = 0.1E_{NO}$) in emissions:

$$S^{(1)} = [C(+\Delta\epsilon) - C(-\Delta\epsilon)]/2\Delta\epsilon \qquad (14)$$

DDM-3D calculations follow the brute-force sensitivities closely. Note that in Figure 2a, NO-inhibited photochemical regime around major urban areas is characterized by negative sensitivity coefficient of ozone to NO emissions and that for the time shown, most of the domain (with the exception of the NO_x-rich plumes of the Bay area and Sacramento) are in NO_x-limited regime.

Figure 2b shows the distribution of the HDDM second-order sensitivity coefficients of ozone concentration with respect to domain-wide NO emissions as well as the field calculated using the brute-force approach:

$$S^{(2)} = [C(+\Delta\epsilon) - 2C(0) + C(-\Delta\epsilon)]/(\Delta\epsilon)^2 \qquad (15)$$

Second-order derivatives are shown for the same time as the first-order coefficients in Figure 2a, again with very good agreement between brute-force and HDDM. Figure 2c,d shows the same comparison (at the same time) for first- and second-order coefficients with respect to domain-wide VOC emissions. The agreement for this sensitivity parameter is very good as well. As expected, first-order sensitivity to VOC emissions is positive at most of the locations in the domain, and second-order coefficients indicate a predominantly concave ozone response. Comparing Figure 2b,d confirms that ozone behaves more linearly in response to changes in VOC emissions than NO_x, as shown by the lower magnitude of the second-order coefficients for VOC emissions. However, the similar spatial distribution in both cases suggests that the same parameter (chemical regime with regard to NO_x availability) controls the nonlinear behavior.

Another type of comparison between HDDM and brute-force coefficients is shown in Figure 3. The plots show the agreement for all grid cells at the time of episode's peak ozone concentration and for first- and second-order sensitivity coefficients to domain-wide NO and VOC emissions. The agreement for all cases is very good, and the slopes are close to one. The accuracy of the results is comparable to a recent regional DDM application (*23*). Note that DDM-3D

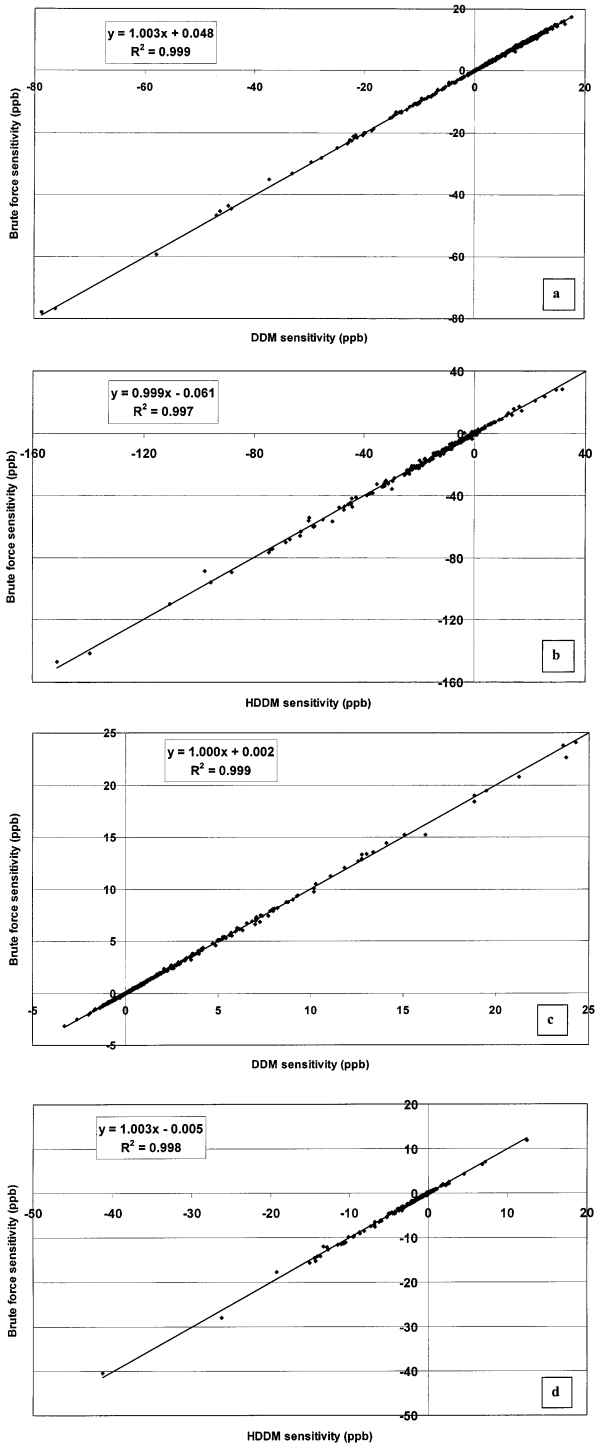

FIGURE 3. Comparison of (H)DDM vs brute-force ozone sensitivity coefficients: (a) first-order to domain-wide NO emissions, (b) second-order to domain-wide NO emissions, (c) first-order to domain-wide VOC emissions, and (d) second-order to domain-wide VOC emissions. All the plots are made for the time of episode's peak ozone concentration (3−4 p.m. on August 2nd). Brute-force coefficients are calculated using a central difference approximation and 10% perturbation (±) in domain-wide NO or VOC emissions.

(and therefore, HDDM as implemented here) is inherently less accurate than the conventional DDM, as in a tradeoff of accuracy for computational efficiency, it integrates the sensitivities in longer time steps than concentration calculations require. Our results in this study show that for most

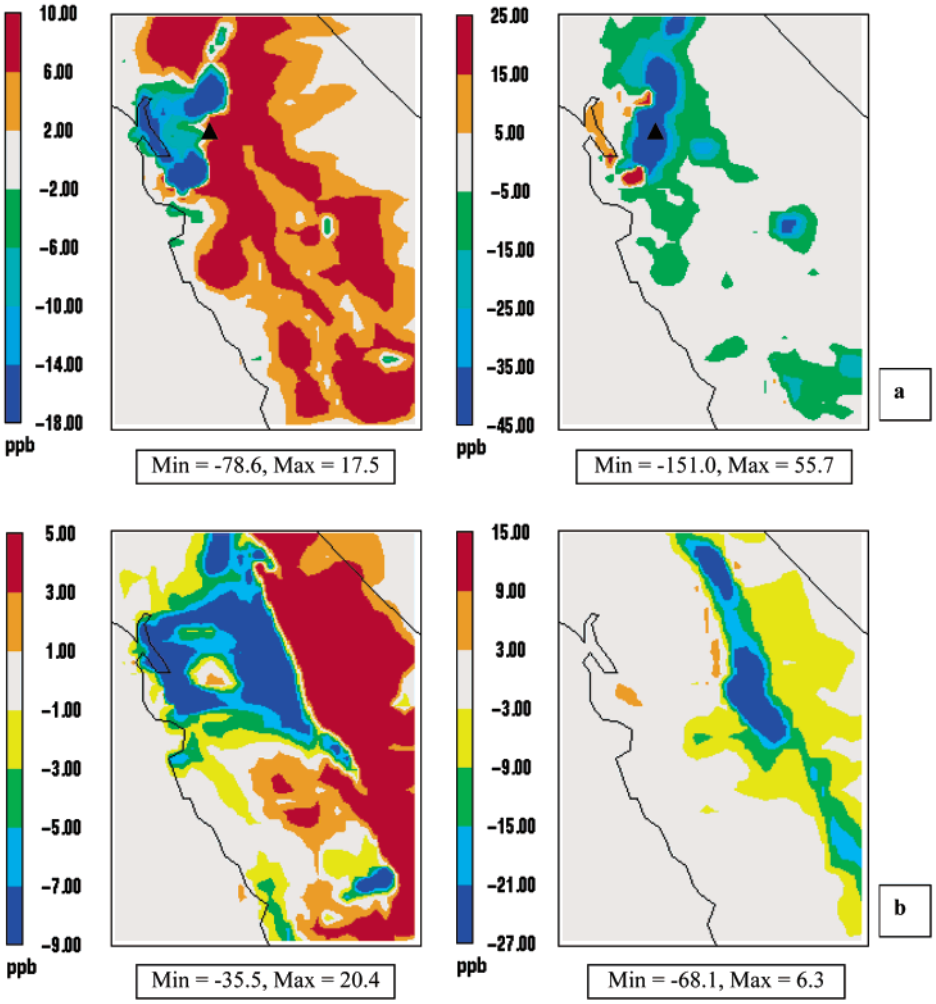

FIGURE 4. A comparison between spatial distributions of first- (left) and second- (right) order sensitivity coefficients of ozone to domain-wide NO emissions: (a) at the time of episode's peak ozone concentration and (b) nighttime (9−10 p.m. local time, August 3rd). The most nonlinear response is seen in areas where a change in chemical regime occurs, i.e., where there is sharp negative to positive gradient in the first-order coefficient. The location of peak ozone is marked in Figure 4a.

cases and applications the loss of accuracy in this tradeoff is minimal.

All the brute-force sensitivity coefficients shown in the results are calculated from (±) 10% perturbation in sensitivity parameter. Using larger perturbation results in slightly worse agreement, as higher-order nonlinearities in truncated terms of eqs 14 and 15 become more significant for larger $\Delta\epsilon$. Using smaller (than 10%) perturbation does not improve the agreement with DDM results (as also found in *23*), as numerical noise increases for smaller perturbations.

Figure 4a shows the peak-time (H)DDM first- and second-order sensitivity coefficients, where a concentrated nonlinear behavior in atmospheric response in the polluted plumes (in particular from the Bay area) is clearly observed. These nonlinear areas (indicated by nonzero second-order coefficients) are located at the front of the advected urban air masses, where NO_x-inhibited mixture is making its way into the NO_x-limited environment. The transition between the two chemical regimes is responsible for the highly nonlinear response. The distinction between different chemical regimes is evident in terms of steep negative to positive gradient of the first-order sensitivity coefficients, at the front of the advected air mass. The same behavior is seen in Figure 4b during the night, where the nonlinearity in front of the advected air mass marks the transition from NO-inhibited (negative first derivative) to NO-limited (positive first derivative) chemical regime.

Chemistry is the main source of nonlinearity in the atmospheric response, and NO_x availability is considered the most significant parameter responsible for nonlinear behavior in ozone photochemistry. The effect of NO_x availability on nonlinear behavior is illustrated in Figure 5 for two locations with differing predominant chemical regimes. Figure 5a shows the time series for ozone concentrations and the first- and second-order derivatives with respect to domain-wide NO emissions for a mostly VOC-limited urban area. Negative first-order sensitivity coefficients indicate that the location is almost always NO-inhibited. Ozone response to NO emission is usually concave (i.e., negative second-order sensitivity coefficient), but at the tails of the response curve with low ozone concentration and at very high or very low NO_x environment a convex response is expected. Such convex nonlinearity can be seen on a daily basis for the NO-inhibited (VOC-limited) case of Figure 5a, during the morning hours of low ozone concentration with high NO_x availability (resulting from the morning rush hour emissions). The afternoon rush hour emissions produce a much smaller convex nonlinearity as the ozone concentrations are much higher. The concave nonlinearity peaks about the same time as the concentration and immediately after the environment begins to become less NO_x-inhibited (i.e.

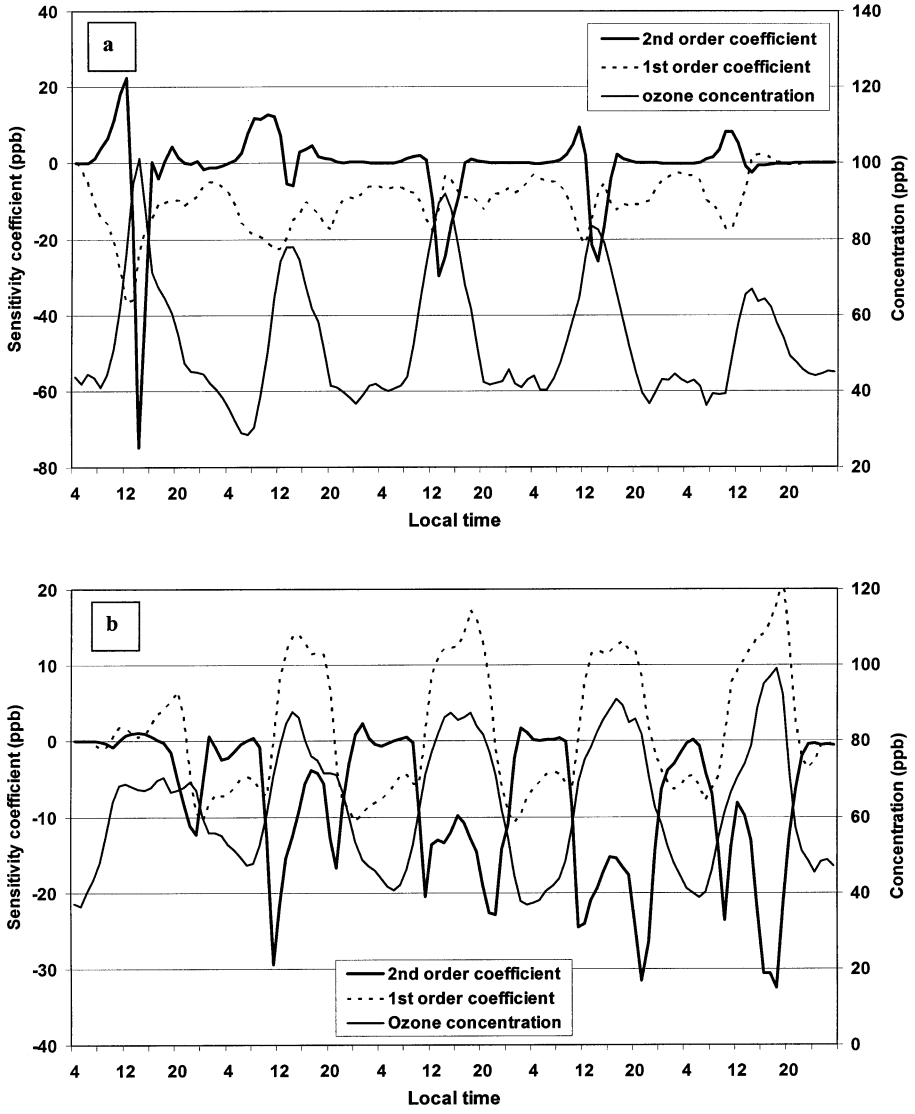

FIGURE 5. Time series of ozone concentration and sensitivity coefficients for a typical (a) VOC-limited urban area and (b) mainly NO_x-limited location.

when the first-order coefficient becomes less negative very early in the afternoon). Figure 5b shows the same time series plots for a location that is mostly NO-limited during the afternoon and early evening but has negative first-order sensitivity to NO emissions during late night and early morning hours. This periodic change in chemical regime results in two distinct daily peaks in the concave nonlinearity. Unlike the case in Figure 5a, the peak nonlinearity does not occur at the same time as the peak concentration but usually happens when the chemical regime changes from NO-inhibited to NO-limited or vice versa, i.e., at the time of sign change in first-order coefficient.

Figure 6 shows spatial distribution of some other higher-order sensitivity coefficients. All the plots are at the time of the daily peak ozone concentration on the second day of the episode. Figure 6a−c shows (H)DDM first-, second-, and third-order sensitivity coefficients of ozone to domain-wide NO emissions. These plots illustrate a general trend where higher-order sensitivity coefficients increase in magnitude (usually with a change in sign) and become more localized. Figure 6d−f shows HDDM second-order sensitivity coefficients to domain-wide VOC emissions, ozone boundary condition, and ozone initial condition, respectively. As expected, the magnitude of nonlinear behavior resulting from VOC emissions is much smaller than that induced by NO emissions (Figure 6b) but both follow a very similar spatial pattern, where nonlinearity is observed at the time and/or location of a change in predominant chemical regime (as shown by sign change in Figure 6a). The boundary condition sensitivity shows the direction of the predominant wind (westerly) and can induce some nonlinearity deep inside the domain. Initial condition sensitivities are gradually dissipated and advected out of the domain, as the simulation progresses. These plots confirm the expectation that, for ozone photochemistry, NO_x emissions trigger the highest magnitude of and most dynamic nonlinear behavior among different sensitivity parameters tested.

One way to test the usefulness of second-order sensitivity coefficients is through Taylor series expansion for a rather large increment:

$$C(+\Delta\epsilon) = C(0) + \Delta\epsilon S^{(1)}(0) + \frac{\Delta\epsilon^2}{2}S^{(2)}(0) + \ldots + \frac{\Delta\epsilon^n}{n!}S^{(n)}(0) + R_{n+1} \quad (16)$$

R_{n+1} is the remainder term of the nth order Taylor series. It should be noted that more accurate methods for parametric extrapolation of physically bounded variables (e.g., concen-

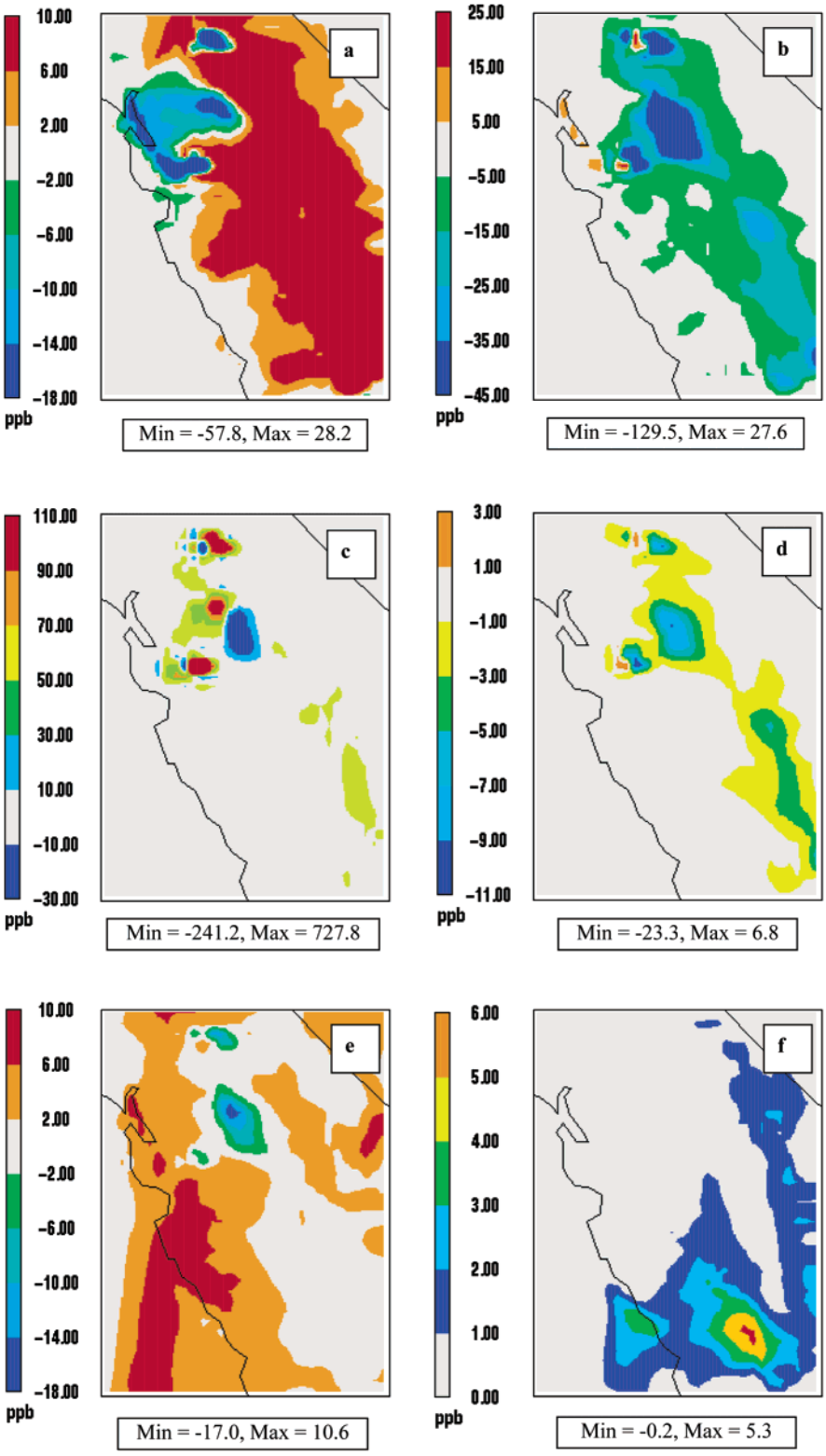

FIGURE 6. HDDM sensitivity coefficients of ozone at the time of daily peak (4 p.m.) on August 3rd: (a) first-order, (b) second-order, and (c) third-order to domain-wide NO emissions; (d) second-order to domain-wide VOC emissions, (e) second-order to ozone boundary condition, and (f) second-order to ozone initial condition.

trations) have been developed (*39*), but Taylor expansion is used here for its simplicity. Figure 7 shows a comparison of the time series of such extrapolation for 50% domain-wide reduction in NO emissions (i.e., $\Delta p = -0.5E_{NO}$, or $\Delta\epsilon = -0.5$), at the location of episode's peak ozone concentration. Simulated results are compared with reconstructed values from first- and second-order Taylor expansion around the base case emission rates. At the time of high ozone concentrations (daily peaks for the first 2 days), second-order prediction is significantly more accurate than linear approximation using the first-order coefficient. At other times, the first-order analysis is accurate in predicting the response. Figure 8 shows the same comparison (as well as the impact of including the third-order coefficient in the Taylor expan-

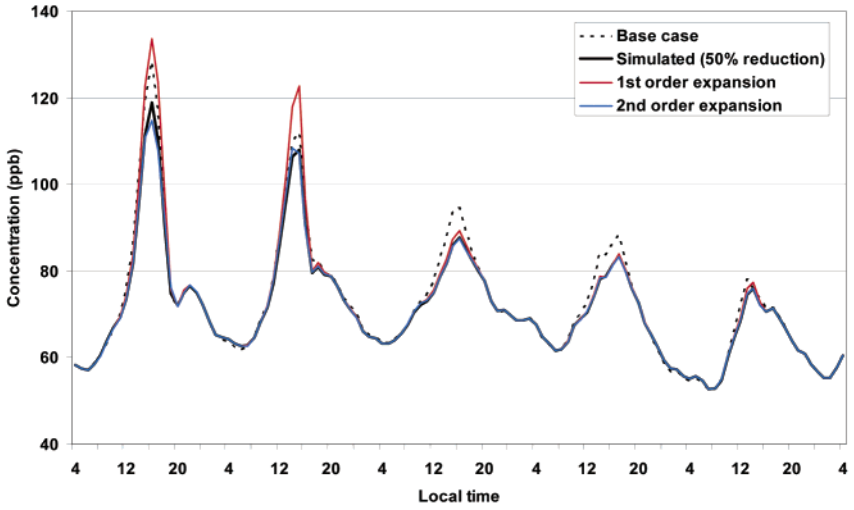

FIGURE 7. Time series of the directly simulated vs Taylor series expanded (predicted from sensitivity coefficients) ozone concentration for a domain-wide 50% reduction in NO emissions at the location of the episode's peak ozone concentration.

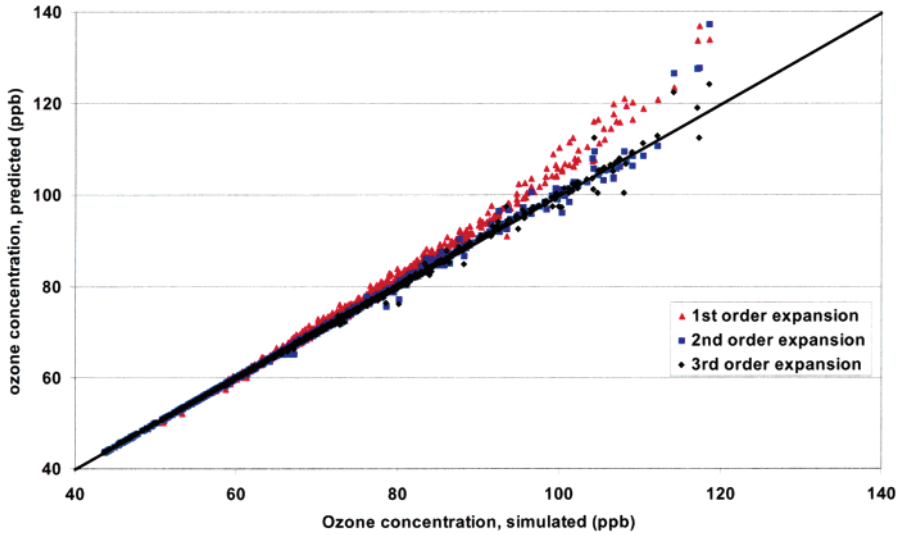

FIGURE 8. Simulated vs predicted (using Taylor expansion) ozone concentration for a domain-wide 50% reduction in NO emissions. Each point represents the concentration at one grid cell at the time of the base case peak ozone on August 3rd. The solid line shows the one-on-one correspondence. Incorporating the higher-order terms in Taylor expansion reduces the prediction error for higher ozone concentrations.

sion) but for all the grid cells and at the time of peak ozone concentration on August 3rd. For most cells in the domain, including higher-order terms in the expansion improves the accuracy. Once again, the improvement is more significant for cells with high ozone concentrations. Figure 9 shows the time series of domain-wide Root Mean Square Error (RMSE) for cells with high ozone concentrations. The accuracy of the ozone prediction is significantly improved by higher-order analysis. It is also important to note that the bulk of the improvement can be achieved by just using the second-order term. In other words, second-order analysis is efficient in capturing most of the nonlinearity in the response.

As mentioned earlier, the computational cost of calculating a higher-order sensitivity coefficient is very close to first-order calculation, and, therefore, the computational efficiency is comparable to first-order sensitivity analysis (*18*, *19*). The main difference is that in eq 11 (or 13) there are more terms to be evaluated on the right-hand side. This difference is small compared to the computational cost associated with the matrix factorization and transport-related computations. Table 1 shows a summary of the relative computational times for different numbers and types of sensitivity parameters. Similar to the case of first-order analysis, calculating a larger number of sensitivity coefficients, all at the same time, reduces the computational overhead, as matrix factorization is shared for all parameters. The Rosenbrock solver is computationally more expensive than the hybrid solver and, therefore, has a smaller relative computational time for sensitivity analysis. This exemplifies two benefits of using DDM-3D. First, changing chemical solvers (e.g., to the more accurate Rosenbrock solver) does not require recoding. Second, implementation of a more expensive (and presumably more accurate) solver does not increase computational overhead for sensitivity calculations.

It should be noted that there is an indirect cost associated with calculation of a higher-order coefficient, as all the lower-order derivatives should also be calculated. On the other hand, calculation of those coefficients using a brute-force method needs more than one simulation (the exact number of which depends on the order as well as combination of the coefficients to be calculated). As the number of sensitivity coefficients (including cross-sensitivities) rapidly increases

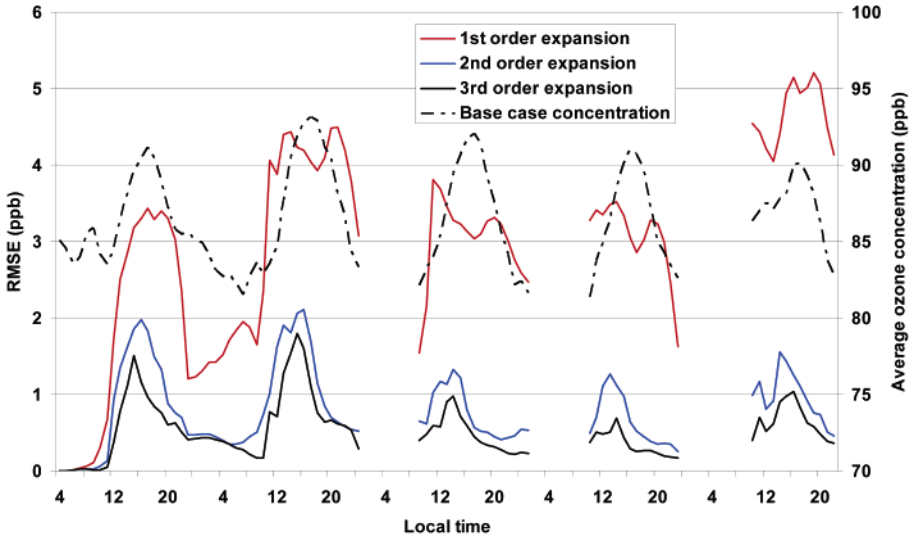

FIGURE 9. Time series of the domain-wide Root Mean Square Error (RMSE) in prediction by Taylor expansion for cells with high (base case) ozone concentration (>80 ppb). Discontinuity in the series represents the hours where less than 10 cells in the domain had ozone concentrations greater than 80 ppb.

TABLE 1: Sensitivity Computational Times Normalized to the Computational Time for the Base Case Concentration Simulation[a]

	Rosenbrock solver	Hybrid solver
concentration only[b]	0.000	0.000
1 sensitivity parameter[c] (first-order)	0.349	0.727
10 sensitivity parameters[c] (first-order)	0.089	0.186
10 sensitivity parameters[c] (five first-order and five second-order parameters)	0.093	0.195
20 sensitivity parameters[d] (first-order)	0.072	0.150

[a] All the values are calculated based on the 5-day simulation times using a 750 MHz SunBlade-1000 workstation. [b] Base case 5-day simulation time was 242 min for the hybrid version, and 505 min for the Rosenbrock version. [c] Sensitivity to the emission rates. [d] Sensitivity to the emission rates (*10*), boundary conditions (*5*), and initial conditions (*5*).

with the order, calculating the coefficients of a large order and/or for many sensitivity parameters can prove to be computationally challenging. HDDM provides a promising approach for higher-order sensitivity analysis as it calculates higher-order coefficients with similar computational efficiency as the first-order coefficients. In addition, second-order analysis appears to be sufficiently effective in describing the nonlinearities encountered in air quality modeling.

Calculation of second- (and/or higher) order sensitivity coefficients can have numerous practical applications. One such application is a higher-order Taylor expansion, similar to the exercise shown in this paper. Taylor series reconstruction of scenario-based modeling cases is a strong policy analysis tool. One particularly useful example is the time and location dependent reconstruction of ozone isopleths for a modeling domain. Another application of higher-order sensitivity calculations is to efficiently quantify uncertainties associated with the first-order derivatives. Uncertainties in the first-order derivative can be of importance because control strategies are devised based on these uncertain values. Uncertainty analysis of organic reactivities is another particularly important example of this application. Second-order sensitivity coefficients may also be used for iterative optimization procedures of nonlinear systems, where direct calculation of sensitivity coefficients is performed, for example, when assessing emission inventory accuracy (*11*). With the use of second-order coefficients, the calculations can be carried out with fewer iterations, and the global optimum can be found more readily.

Acknowledgments

This work was supported by the California Air Resources Board and the Georgia Power Company.

Literature Cited

(1) Seigneur, C.; Tesche, T. W.; Roth, P. M.; Reid, L. E. *J. Appl. Meteorol.* **1981**, *20*, 1020−1040.
(2) Gao, D.; Stockwell, W. R.; Milford, J. B. *J. Geophys. Res.* **1996**, *101*, 9107−9119.
(3) Russell, A. G.; Milford, J.; Bergin, M. S.; McBride, S.; McNair, L.; Yang, Y.; Stockwell, W. R.; Croes, B. *Science* **1995**, *269*, 491−495.
(4) Bergin, M. S.; Russell, A. G.; Milford, J. B. *Environ. Sci. Technol.* **1995**, *29*, 3029−3037.
(5) Hwang, J.-T.; Dougherty, E. P.; Rabitz, S.; Rabitz, H. *J. Chem. Phys.* **1978**, *69*, 5180−5191.
(6) Dougherty, E. P.; Hwang, J.-T.; Rabitz, H. *J. Chem. Phys.* **1979**, *71*, 1794−1808.
(7) Kramer, M. A.; Rabitz, H.; Calo, J. M.; Kee, R. J. *Int. J. Chem. Kinet.* **1984**, *16*, 559−578.
(8) Kramer, M. A.; Calo, J. M.; Rabitz, H. *Appl. Math. Modell.* **1981**, *5*, 432−441.
(9) Bischof, C. A.; Carle, A.; Corliss, G.; Griewank, A.; Hovland, P. *Sci. Prog.* **1992**, *1*, 11−29.
(10) Carmichael, G. R.; Sandu, A.; Potra, F. A. *Atmos. Environ.* **1997**, *31*, 475−489.
(11) Hwang, D.; Byun, D. W.; Odman, M. T. *Atmos. Environ.* **1997**, *31*, 879−888.
(12) Dickerson, R. R.; Stedman, D. H.; Delany, A. C. *J. Geophys. Res.* **1982**, *87*, 4933−4942.
(13) Dunker, A. M. *Atmos. Environ.* **1981**, *15*, 1155−1161.
(14) Dunker, A. M. *J. Chem. Phys.* **1984**, *81*, 2385−2393.
(15) Milford, J. B.; Gao, D.; Russell, A. G.; McRae, G. J. *Environ. Sci. Technol.* **1992**, *26*, 1179−1189.
(16) Gao, D.; Stockwell, W. R.; Milford, J. B. *J. Geophys. Res.* **1995**, *100*, 23153−23166.
(17) Seefeld, S.; Stockwell, W. R. *Atmos. Environ.* **1999**, *33*, 2941−2953.
(18) Yang, Y.-J.; Wilkinson, J. G.; Russell, A. G. *Environ. Sci. Technol.* **1997**, *31*, 2859−2868.
(19) Mendoza-Dominguez, A.; Russell, A. G. *Environ. Sci. Technol.* **2000**, *34*, 4974−4981.
(20) Boylan, J. W.; Odman, M. T.; Wilkinson, J. G.; Russell, A. G.; Yang, Y.-J.; Mueller, S. F.; Imhoff, R. 2003, submitted for publication.
(21) Hakami, A.; Harley, R. A.; Milford, J. B.; Odman, M. T.; Russell, A. G. 2003, submitted for publication.
(22) Dunker, A. M.; Yarwood, G.; Ortmann, J. P.; Wilson, G. M. *Environ. Sci. Technol.* **2002**, *36*, 2953−2964.

(23) Dunker, A. M.; Yarwood, G.; Ortmann, J. P.; Wilson, G. M. *Environ. Sci. Technol.* **2002**, *36*, 2965−2976.
(24) Rabitz, H.; Kramer, M. A.; Dacol, D. *Annu. Rev. Phys. Chem.* **1983**, *34*, 419−461.
(25) Guay, M.; McLean, D. D. *Comput. Chem. Eng.* **1995**, *19*, 1271−1285.
(26) Dunker, A. M. *Atmos. Environ.* **1986**, *20*, 479−486.
(27) Glasson, W. A.; Dunker, A. M. *Environ. Sci. Technol.* **1989**, *23*, 970−978.
(28) Vuilleumier, L.; Harley, R. A.; Brown, N. J. *Environ. Sci. Technol.* **1997**, *31*, 1206−1217.
(29) Odman, M. T.; Ingram, C. L. *Multiscale Air Quality Simulation Platform (MAQSIP): Source Code Documentation and Validation;* Technical Report, MCNC; North Carolina Supercomputing Center: Research Triangle Park, NC, 1996.
(30) DaMassa, J.; Tanrikulu, S.; Magliano, K.; Ranzieri, A. J.; Niccum, L. *Performance Evaluation of SAQM in Central California and Attainment Demonstration for The August 3−6, 1990 Ozone Episode;* California Air Resources Board: CA, 1996.
(31) McRae, G. J.; Goodin, W. R.; Seinfeld, J. H. *Atmos. Environ.* **1982**, *16*, 679−696.
(32) Gery, M. W.; Whitten, G. Z.; Killus, J. P.; Dodge, M. C. *J. Geophys. Res.* **1989**, *94*, 12925−12956.
(33) Bott. A. *Mon. Wea. Rev.* **1989**, *117*, 1006−1015.
(34) Young, T. R.; Boris, J. P. *J. Phys. Chem.* **1977**, *81*, 2424−2427.
(35) Hesstvedt, E.; Hov, O.; Isaksen, I. S. A. *Int. J. Chem. Kinetics* **1978**, *10*, 971−994.
(36) Hairer, E.; Wanner, G. *Solving Ordinary Differential Equations II. Stiff and Differential-Algebraic Problems*; Springer-Verlag: Berlin, 1991.
(37) Sandu. A.; Verwer, J. G.; Blom, J. G.; Spee, E. J.; Carmichael, G. R.; Potra, F. A. *Atmos. Environ.* **1997**, *31*, 3459−3472.
(38) Harley, R. A.; Russell, A. G.; McRae, G. J.; Cass, G. R.; Seinfeld, J. H.; *Environ. Sci. Technol.* **1993**, *27*, 378−388.
(39) Kramer, M. A.; Rabitz, H.; Calo, J. M. *Appl. Math. Modell.* **1984**, *8*, 341−350.

Received for review April 5, 2002. Revised manuscript received March 17, 2003. Accepted March 21, 2003.

ES020677H